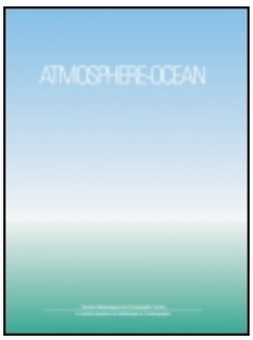

Atmosphere-Ocean

ISSN: 0705-5900 (Print) 1480-9214 (Online) Journal homepage: http://www.tandfonline.com/loi/tato20

Parametrization schemes of incident radiation in the North Water polynya

J.M. Hanesiak , D.G. Barber , T.N. Papakyriakou & P.J. Minnett

To cite this article: J.M. Hanesiak , D.G. Barber , T.N. Papakyriakou & P.J. Minnett (2001) Parametrization schemes of incident radiation in the North Water polynya, Atmosphere-Ocean, 39:3, 223-238, DOI: 10.1080/07055900.2001.9649678

To link to this article: http://dx.doi.org/10.1080/07055900.2001.9649678

Parametrization Schemes of Incident Radiation in the North Water Polynya

J.M. Hanesiak[1]*, D.G. Barber[1], T.N. Papakyriakou[1] and P.J. Minnett[2]

[1]*Centre for Earth Observation Science, Geography Department, University of Manitoba, Winnipeg, MB R3T 2N2*

[2]*Meteorology and Physical Oceanography Division, Rosenstiel School of Marine and Atmospheric Science, University of Miami, Miami, Florida, U.S.A.*

[Original manuscript received 16 December 1999; in revised form 28 September 2000]

ABSTRACT *Surface incident radiation is a critical component of the Arctic surface energy balance making it important for sea-ice model parametrizations to properly account for these fluxes. In this article, we test the performance of various incident short-wave (K↓) and long-wave (L↓) flux parametrizations using unique observations from the 1998 International North Water (NOW) Polynya Project between March and July. The dataset includes hourly observations over terrestrial, fast-ice and full marine polynya environments allowing for parametrization comparisons between each environment and determination of any seasonal biases. Performance testing is highly dependent on observed input parameters that contain relative errors, however, significant differences between the marine and fast-ice fluxes are evident. Results are very similar between the terrestrial and fast-ice sites. The best K↓ clear-sky schemes underestimate fluxes in the colder season and overestimate them in the warm season, with greater biases in the marine setting. The K↓ cloudy-sky results suggest a similar cold and warm season bias but with greater magnitudes, especially in the marine environment. The K↓ cloudy-sky schemes require seasonal improvements, especially in the marine atmosphere. The L↓ clear-sky fluxes were generally overestimated during the colder season. Accounting for a less emissive atmosphere resulted in better flux approximations in all environments. L↓ cloudy-sky fluxes were generally underestimated. Adjusting the cloudy-sky emissivity improved the estimated fluxes, however, results were very different in the marine setting. The L↓ cloudy-sky parametrizations may require re-evaluation due to a consistent negative bias as the observed flux increases.*

RÉSUMÉ *[Traduit par la rédaction] Le rayonnement incident à la surface est l'un des principaux facteurs du bilan énergétique de la surface dans l'Arctique, et c'est pourquoi il est important que ces flux soit adéquatement paramétrisés dans les modèles de glaces de mer. Dans cet article, nous évaluons la performance de diverses paramétrisations des flux incidents d'ondes courtes (K↓) et d'ondes longues (L↓), au moyen des observations (les seules du genre) effectuées entre mars et juillet dans le cadre du Programme international de la polynie des eaux du Nord de 1998. L'ensemble de données comprend des observations horaires faites dans des environnements terrestre, de banquise côtière et de polynie marine, qui permettent de comparer les paramétrisations dans chacun de ces environnements et de déterminer les biais saisonniers. Bien que l'évaluation de la performance dépende grandement des paramètres d'entrée observés qui contiennent des erreurs relatives, on relève des différences importantes entre les flux marins et de banquise côtière. Les résultats sont très semblables entre les sites terrestres et les sites de banquise côtière. Les meilleurs schémas de K↓ par ciel clair sous-estiment les flux durant la saison la plus froide et les surestiment durant la saison chaude, les biais les plus marqués étant observés en milieu marin. Les résultats pour K↓ par ciel nuageux montrent aussi des biais durant les saisons froide et chaude, mais avec de plus grandes amplitudes, surtout dans l'environnement marin. Les schémas de K↓ par ciel nuageux requièrent des améliorations en fonction de la saison, surtout dans l'atmosphère marine. Les flux L↓ par ciel clair sont généralement surestimés durant la saison la plus froide. La prise en compte d'une atmosphère moins émissive donne de meilleures approximations de flux dans tous les environnements. Les flux L↓ par ciel nuageux sont généralement sous-estimés. L'ajustement de l'émissivité par ciel nuageux améliore les flux estimés, mais les résultats sont néanmoins très différents en milieu marin. Il faudrait peut-être réévaluer les paramétrisations de L↓ par ciel nuageux, étant donné un biais négatif constant quand le flux observé augmente.*

1 Introduction

We expect to see the first and largest impact of global climate change within the polar regions (IPCC, 1996). Sea ice plays a central role in this change because of a variety of feedback mechanisms which amplify changes within the system (Moritz and Perovich, 1998). These feedback processes occur over a continuum of spatial and temporal scales and already

*Corresponding author's e-mail: john_hanesiak@umanitoba.ca

appear to be linked to a global scale increase in air temperature, as evidenced by: 1) a reduction in sea-ice extent of about 34,000 km^2 per year over the past 18 years (Parkinson et al., 1999); 2) an ice volume decrease of about 40% over the past few decades (Rothrock et al., 1999); and 3) a shift in the principal modes of atmospheric circulation (Walsh et al., 1996). The observed changes in the Arctic marine environment require scientific investigation at a variety of scales using a combination of in situ observations, remote sensing observations and numerical process models.

Thermodynamic sea-ice models offer a powerful tool to help us understand these processes and they can be used in combination with electromagnetic scattering models to produce better estimates of both the geophysical and thermodynamic characteristics of snow-covered sea ice using a multitude of currently available remote sensing platforms (e.g., Jezek et al., 1998; Carsey et al., 1992; Barber and Nghiem, 1999). The one-dimensional thermodynamic sea-ice models offer dual benefits of linking thermodynamics to the surface energy balance with the added benefit of computational simplicity. These types of models are widely used in the sea-ice community (Flato and Brown, 1996; Ebert and Curry, 1993; Hanesiak et al., 1999, to name a few) both to understand the nature of the sea-ice surface energy balance and to link it to the electromagnetic response

Thermodynamic sea-ice models require precise parametrization of the short-wave and long-wave fluxes over a variety of time and space scales. Incident radiation (short-wave ($K\downarrow$) and long-wave ($L\downarrow$)) fluxes are usually two orders of magnitude greater than the oceanic heat flux at the ice underside and planetary boundary layer turbulent fluxes, resulting in radiative fluxes dominating the overall sea-ice surface energy balance. The equilibrium ice thickness of a one-dimensional thermodynamic sea-ice model varies by 4 m for a ±5% change in $K\downarrow$ and 12 m for a similar change in $L\downarrow$ (Ebert and Curry, 1993). The ice pack could completely disappear in summer with an increase in $L\downarrow$ greater than 2% (Ebert and Curry, 1993). $K\downarrow$ is most sensitive to atmospheric aerosol optical depth and humidity under clear skies and cloud optical depth, cloud liquid water content and surface albedo under cloudy skies (Key et al., 1996; Leontyeva and Stamnes, 1993). $L\downarrow$ is most sensitive to precipitable water and aerosol optical depth under clear skies and cloud base height/optical depth for cloudy skies (Key et al., 1996). Dependencies on solar zenith angle (time of day and year) are also critical for assessing the effects of Arctic clouds on net surface heating and cooling (Minnett, 1999; Hanafin and Minnett, this issue). In the absence of an adequate measurement network, accurate simulations of sea-ice thermodynamics require accurate incident radiation parametrizations.

Incident radiative flux parametrization derivation and validation have been limited to mid-latitude oceanic, Arctic land-based, modelling experiments and limited on-ice measurements (see for example, Shine, 1984; Bennett, 1982; Efimova, 1961; Maykut and Church, 1973). Coincident in situ radiation data, comparing different Arctic environments and spatial variations have never previously been available. Data presented here were made in a marine polynya environment including terrestrial, shore fast-ice, marginal ice zone and open water regions during the International North Water (NOW) Polynya Project conducted from March – July 1998 (Barber et al., this issue). The purpose of this article is to: 1) critically assess selected $K\downarrow$ and $L\downarrow$ parametrizations against in situ field measurements and identify seasonal or environmental/spatial biases for these data, and 2) offer improved parametrization representations for the different environments where possible.

Key et. al. (1996) discussed several simple $K\downarrow$ and $L\downarrow$ schemes that performed well in the Arctic that are still used in one-dimensional thermodynamic sea-ice models and two-dimensional dynamic-thermodynamic models (see for example, Flato and Brown, 1996; Maslanik et al., 1995; Ebert and Curry, 1993). Only those parametrizations that were selected to outperform others (by Key et al., 1996) were used in this study. The $K\downarrow$ parametrizations used include Bennett (1982) and Shine (1984) for clear skies and Jacobs (1978) and Shine (1984) for cloudy skies. The $L\downarrow$ parametrizations include Ohmura (1981), Efimova (1961) and Maykut and Church (1973) for clear skies and Jacobs (1978) and Maykut and Church (1973) for cloudy skies. The schemes are attractive for sea-ice modelling due to their simplicity and computational ease and perform fairly well over daily and hourly averages in most cases (Key et al., 1996; Hanesiak et al., 1999). However, their performance can be affected by observational errors in input parameters and unknown total column atmospheric conditions. We refrain from detailed discussions of the various parametrizations in light of Key et al.'s (1996) comprehensive review, and simply outline their empirical formulations.

2 Data and methods

a *Observational Data*

Data collected were from the NOW Polynya Project during an intensive field campaign from March to the end of July 1998 (Barber et al., this issue). The three primary data collection platforms were a terrestrial camp (Cape Herschel) and fast-ice site (Rosse Bay) on the east coast of Ellesmere Island, Nunavut and the Canadian Coast Guard ice-breaker CCGS *Pierre Radisson* in the NOW Polynya region (Fig. 1 and Fig. 2 of Minnett, this issue). Cape Herschel is located 74.67°W, 78.65°N and the fast-ice site was 3.5 km due north of the terrestrial camp. The fast-ice regime was typified by smooth first-year sea ice (Fig. 1; dark shades in Rosse Bay) with a snow cover between 5 and 15 cm up to complete snow melt by early June. The terrestrial site was 100 m AMSL, with a full snow cover and gradual sloping terrain toward Rosse Bay. The fast-ice edge at Cape Herschel was initially 3–4 km off shore and receded to less than 1 km by early June. Measurements of $K\downarrow$ and $L\downarrow$ were available from instruments that were mounted on the foredeck of the CCGS *Pierre Radisson* from transects within the NOW Polynya. Radiation flux densities were measured over several ice types and under

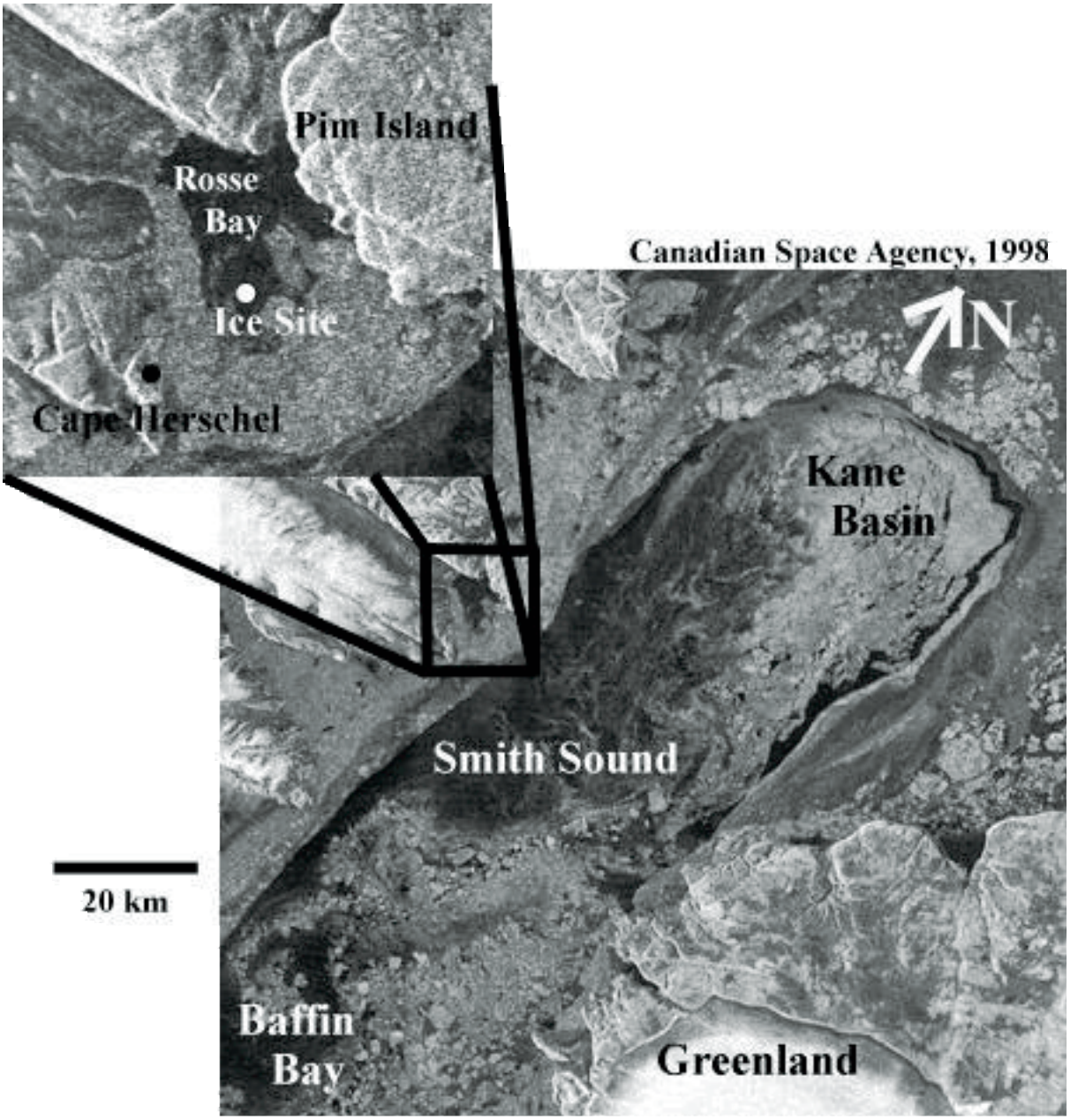

Fig. 1 Geographical locations of the terrestrial camp (Cape Herschel) and ice site in Rosse Bay during the 1998 International (NOW) Polynya project. Image is a synthetic aperture radar (SAR) image from Radarsat-1 (© Canadian Space Agency, 1998). Dark shades represent smooth first-year ice in Rosse Bay and open water in Smith Sound. The ice bridge at the north end of the polynya is denoted for reference.

a variety of atmospheric conditions. Data were measured every second and stored as one-minute averages. The terrestrial and ice camps were operational between Year-Day (YD) 89 (30 March) and YD155 (4 June) and the ice-breaker between approximately YD99 (9 April) to YD203 (22 July). This resulted in 601 h and 822 h of useful terrestrial site $K\downarrow$ and $L\downarrow$ data, respectively, 635 h and 915 h at the fast-ice site and 659 h and 988 h on the ice-breaker. There were less short-wave hours due to night-time darkness in the early spring and data quality control (see below).

Incident short-wave and long-wave radiation were sampled every 5 s by an Eppley pyranometer (model PSP) and pyrgeometer (model PIR) which were installed at both the Cape Herschel and Rosse Bay sites. The radiometers were mounted 1.2 m above the surface and recorded 15-min radiation averages. Incident short-wave and long-wave radiation were measured using Eppley 8-48 "Black and White" Pyranometers on the ice-breaker, and pyrgeometers (model PIR) mounted on gimbles 6 m above the ship's deck to ensure proper levelling in the mean. Measurement accuracy is estimated at ±10 W m^{-2} and ±2.5% for the pyrgeometers (Philipona et al., 1995) and pyranometers (Latimer, 1972), respectively. The spectral response of the PSP and 8-48 pyranometers is determined by the glass dome over the sensors,

which has uniform transmission for radiation in the wavelength range 0.285 to 2.8 μm. The spectral response of the PIR, determined by an interference filter inside a silicon dome, ranges from 3.5 to 50 μm. To sample $K\uparrow$, a down-facing pyranometer (Eppley, model PSP) was installed on a scaffold-type tower 2.55 m above the fast-ice surface and another down-facing pyranometer (Eppley 8-48) was intalled on the bow of the CCGS *Pierre Radisson* extending 3 m out. These radiation instruments are designed to measure the critical wavelengths of the solar and infra-red spectra that control radiative fluxes. Supplementary hourly data included air temperature (T) (error approximately ±0.1°C), relative humidity (RH) (error ± 5%), total cloud fraction (c) (error ± 10%), and surface albedo (± 0.03 albedo units) used as input for the radiative flux parametrizations (discussed below). T and RH were measured 2 m above the surface at Cape Herschel using a relative humidity probe (CSI 207F) and 15 m above the water line of the ship. Surface albedo was estimated as the ratio of $K\uparrow$ to $K\downarrow$ at the Rosse Bay site and from the CCGS *Pierre Radisson.* Short-wave albedo estimates were continuous and stable at Rosse Bay, but intermittent on the ice-breaker due to rime build-up on the sensor. Total cloud fractions were determined from hourly observations at the terrestrial/fast-ice sites taken by on-site personnel and an all-sky time lapse video camera on the ship. The all-sky camera is an all-weather camera looking downward on a hemispheric mirror that produces a 180° view of the celestial dome. Hourly averages of total cloud fraction were determined from analyses of the video images sub-sampled at 10-minute intervals. A discussion of the cloud conditions is given elsewhere in this volume (Hanafin and Minnett, this issue). Incident radiation was measured over the temperature range –30°C to +3°C from late winter to early summer at the terrestrial and fast-ice sites and –8°C to +12°C on the ice-breaker. As a result, there was little overlap of temperature and vapour pressure between the fast-ice and ice-breaker measurements (i.e., the two environmental regimes were quite different).

Data were stratified into clear-sky (0- to 1-tenth coverage) and all-sky (2 to 10-tenths coverage) conditions, solar zenith angle (Z), and location (terrestrial, fast-ice, ice-breaker). Seasonal variations according to air temperature were also investigated for parametrization seasonal biases. Clear-sky data were combined into 0- to 1-tenth sky cover since there was no difference between the mean short-wave and long-wave radiative fluxes associated with them. This resulted from hourly averaging and the little time the solar disk was obscured by very few cumulus clouds. The Z is used as an independent variable since some parametrizations have been shown to contain Z biases (Key et al., 1996). In addition, all $K\downarrow$ data with a $Z > 75°$ were omitted due to measurement error at these angles, especially albedo ($K\uparrow$ fluxes). Location stratification was performed for parametrization performance between the terrestrial, fast-ice and full marine environments. The fast-ice and terrestrial datasets are more accurate due to their stable measurement platforms and less prone to the harsh marine environment; they show smaller errors between the observed and estimated fluxes (see below).

b *Radiative Flux Parametrizations*

The parametrizations have been categorized into clear-sky and all-sky fluxes with similar conventions as in Key et al. (1996), for consistency. The downwelling short-wave flux ($K\downarrow$), downwelling long-wave flux ($L\downarrow$) and solar constant (S = 1356) are in W m^{-2}; solar zenith angle (termed Z above) is in degrees, near surface air temperature (T) is in Kelvin, near-surface vapour pressure (ea) in hPa, cloud fraction (c), cloud optical depth (τ), and surface albedo (α). A more detailed discussion of each parametrization can be found in Key et al. (1996). A brief description of each parametrization is outlined.

1 SHORT-WAVE CLEAR SKY FLUX

Key et al. (1996) indicated that the best clear sky $K\downarrow$ ($K\downarrow_{clr}$) parametrization in their study was that of Shine (1984) with Bennett (1982) performing reasonably well over daily averages. The Shine (1984) parametrization attempts to account for the near surface vapour pressure explicitly and was tested with a radiative transfer model. In comparison, the scheme of Bennett (1982) is less comprehensive and is primarily intended for the estimation of mean monthly values.

The form of Bennett (1982) for $K\downarrow_{clr}$ is

$$K\downarrow_{clr} = 0.72\ S\cos(Z). \tag{1}$$

The form of Shine (1984) for $K\downarrow_{clr}$ is

$$K\downarrow_{clr} = (S\cos^2(Z)) / [1.2\cos(Z) + (1.0 + \cos(Z)) \times 10^{-3}\ ea + 0.0455]. \tag{2}$$

2 SHORT-WAVE ALL-SKY FLUX

To parametrize cloud effects on the all-sky $K\downarrow$ flux, two approaches were found to perform reasonably well. One is simply to multiply the clear sky flux by a function of cloud fraction as in Jacobs (1978). Another, more sophisticated, approach is to account for surface changes (or albedo changes) affecting multiple reflections between the surface and cloud as well as cloud properties (or optical depth/thickness) as in Shine (1984) that performs well over shorter time periods (Key et al., 1996). We assume a constant cloud optical thickness (7.0) according to Ebert and Curry (1993) and input the computed hourly surface albedo from the Rosse Bay and ice-breaker platforms.

The form of Jacobs (1978) under all-sky conditions is

$$K\downarrow_{all} = K\downarrow_{clr}(1 - 0.33\ c). \tag{3}$$

The form of Shine (1984) under all-sky conditions is

$$K\downarrow_{cld} = (53.5 + 1274.5\cos(Z))\cos^{0.5}(Z) / [1 + 0.139\ (1 - 0.9345\ \alpha)\ \tau]. \tag{4a}$$

$$K\downarrow_{all} = (1 - c)\, K\downarrow_{clr} + c\, K\downarrow_{cld}. \quad (4b)$$

3 CLEAR SKY LONG-WAVE FLUX

Down-welling clear-sky long-wave radiation ($L\downarrow_{clr}$) is typically a function of near-surface temperature and vapour pressure. Three commonly used parametrizations differ in their treatment of the atmospheric emittance. Ohmura (1981) considers the atmospheric emittance as a function of near-surface air temperature. Maykut and Church (1973), on the other hand, assign a constant value to the atmospheric emittance, and Efimova (1961) makes the term a function of near-surface temperature and vapour pressure.

The form of Ohmura (1981) for $L\downarrow_{clr}$ is

$$L\downarrow_{clr} = \sigma\, T^4\, (8.733 \times 10^{-3}\, T^{0.788}). \quad (5)$$

The form of Maykut and Church (1973) for $L\downarrow_{clr}$ is

$$L\downarrow_{clr} = 0.7855\, \sigma\, T^4. \quad (6)$$

The form of Efimova (1961) for $L\downarrow_{clr}$ is

$$L\downarrow_{clr} = \sigma\, T^4\, (0.746 + 0.0066\, ea). \quad (7)$$

4 ALL-SKY LONG-WAVE FLUX

An increase in $L\downarrow$ associated with clouds is a function of cloud fraction in expressions derived by Jacobs (1978) and Maykut and Church (1973). Jacobs (1978) developed a simple linear relationship between cloud emittance, cloud fraction and the clear-sky flux, while the relationship of Maykut and Church (1973) is exponential in form. Cloud emissivity also differs between the two formulations.

The form of Jacobs (1978) $L\downarrow_{all}$ is

$$L\downarrow_{all} = L\downarrow_{clr}\, (1 + 0.26\, c). \quad (8)$$

The form of Maykut and Church (1973) $L\downarrow_{all}$ is

$$L\downarrow_{all} = L\downarrow_{clr}\, (1 + 0.22\, c^{2.75}). \quad (9)$$

c *Analysis Methods*

The $K\downarrow_{clr}$ and $L\downarrow_{clr}$ schemes were individually tested. The all-sky $K\downarrow$ and $L\downarrow$ parametrizations require a clear-sky component, hence different combinations of the various schemes were performed. The $K\downarrow$ all-sky combinations included: 1) the clear-sky of Shine with the cloudy sky correction of Shine, 2) the clear-sky of Bennett with the cloudy-sky correction of Jacobs, 3) the clear-sky of Shine with the cloudy-sky correction of Jacobs, and 4) the clear-sky of Bennett with the cloudy-sky correction of Shine. The $L\downarrow$ all-sky combinations included: 1) the clear-sky of Maykut-Church (MC) with the cloudy-sky correction of MC, 2) the clear-sky of Ohmura with the cloudy-sky correction of Jacobs, 3) the clear-sky of Efimova with the cloudy-sky correction of Jacobs, 4) the clear-sky of MC with the cloudy-sky correction of Jacobs, and 5) the clear-sky of Efimova with the cloudy-sky correction of MC.

The radiation and meteorological data were converted to hourly averages (centred on the hour). The supplementary meteorological data from each observing platform was used as input for the parametrizations. The difference between the modelled and observed flux (difference parameter) was used to measure the performance of each scheme. Performance was quantified using statistical indices on the difference parameter such as simple linear regression tests for biases, mean bias error (MBE) and the root-mean-square error (RMSE). The linear slope of regression lines fitted along the difference parameter were statistically tested with an associated confidence interval to infer significant biases (slope significantly different from the mean) as functions of solar zenith angle (Z), season and the type of environment. Residual plots revealed that a linear model is appropriate for each regression line along the difference parameter.

For the seasonal bias analysis, the observed and estimated radiation were stratified into temperature regimes. The measured and estimated fluxes were binned according to the following temperature categories: (1) $T \le -20$°C, (2) -20°C $< T \le -14$°C, (3) -14°C $< T \le -9$°C, (4) -9°C $< T \le -2$°C, and (5) $T > -2$°C. The categories correspond to the main 'seasonal' transitory atmospheric and sea-ice conditions for the NOW region (Hanesiak, 1998) and allow enough statistically viable data points for the comparisons in each temperature regime.

3 Results — parametrizations vs. observations

a *Terrestrial and Fast-Ice Sites*

The results from the analysis using data from the terrestrial and fast-ice sites were similar (generally within 2%). Consequently the following sections describe the performance of the models from the fast-ice site.

1 INCIDENT SHORT-WAVE FLUXES

Our results are in agreement with Key et al. (1996) showing that the Shine scheme is preferable to Bennett's equation (Fig. 2 and Table 1). The Bennett scheme contains a negative Z bias with decreasing Z (Fig. 2) within a 99% confidence interval. The Shine scheme performs well for the fast-ice dataset with only 1.1 W m^{-2} mean error (5.0 W m^{-2} at the terrestrial site). The parametrization statistics in Table 1 are slightly better than Key et al. (1996). The cancellation of errors between negative and positive values may contribute to the low mean errors.

For the $K\downarrow$ all-sky combinations our results again support Key et al. (1996). The error statistics (Table 2) and error plots (Fig. 3) show that the best parametrization combination is Shine/Shine with a mean error of –2.1 W m^{-2} (3.1 W m^{-2} at the terrestrial site). The Jacobs cloudy-sky scheme depletes too much radiation when combined with the Shine and Bennett clear-sky routines, shown by the highly negative mean errors.

2 INCIDENT LONG-WAVE FLUXES

The parametrization of Ohmura performs better than both MC's and Efimova's schemes (Table 3). Key et al. (1996)

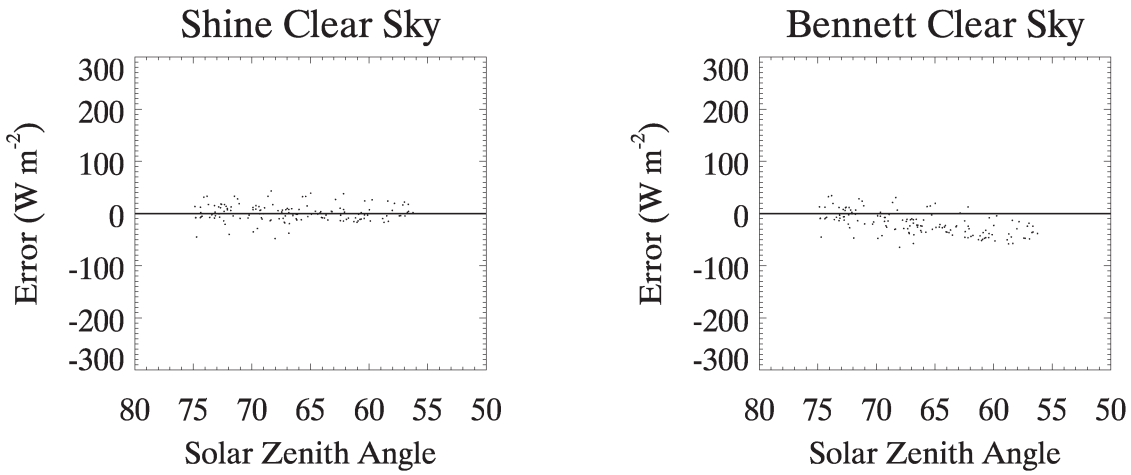

Fig. 2 The clear-sky short-wave flux error for two parametrizations (modelled flux minus the observed flux at Rosse Bay).

TABLE 1. Parametrized clear-sky short-wave flux error (estimated flux minus the measured fast-ice flux). Bracketed values are the corresponding ice-breaker results. The mean, mean error and RMSE are in W m^{-2}. The number of observations is also shown.

No. obs = 145(104)	Mean	R^2	Mean Error	RMSE
Observed	391.9(419.1)	–	–	–
Shine	393.1(442.9)	0.99(0.91)	1.1(23.9)	15.9(48.8)
Bennett	373.1(426.3)	0.98(0.91)	–18.8(7.3)	21.6(47.8)

TABLE 2. Parametrized all-sky short-wave flux error (estimated flux minus the measured fast-ice flux). Bracketed values are the corresponding ice-breaker results. The mean, mean error and RMSE are in W m^{-2}. The number of observations is also shown.

No. obs = 456(555)	Mean	R^2	Mean Error	RMSE
Observed	322.4(250.7)	–	–	–
Shine/Shine	320.3(332.4)	0.83(0.76)	–2.1(81.7)	59.6(90.1)
Bennett/Jacobs	289.9(351.0)	0.85(0.71)	–32.4(100.3)	60.6(95.9)
Shine/Jacobs	304.0(370.1)	0.85(0.71)	–18.4(119.4)	57.9(96.5)
Bennett/Shine	315.1(322.5)	0.82(0.75)	–7.4(71.8)	61.3(90.8)

found the Efimova routine to perform best. The emittance of long-wave radiation is too high in both MC's and Efimova's schemes for incident fluxes less than about 240 W m^{-2}. A similar trend is shown by Key for the MC model. If the clear-sky atmospheric emissivity is adjusted by roughly the same amount in MC (from 0.7855 to 0.729) and Efimova (0.746 to 0.7; the first coefficient independent of vapour pressure) during periods of low emittance ($L\downarrow$ < 240 W m^{-2}) the results from both parametrizations improve (Table 4 and Fig. 4). The emissivities for each scheme were optimized to fit our data by minimizing the MBE for each scheme.

For the $L\downarrow$ all-sky combinations, Efimova/MC had both the smallest MBE and RMSE of the combinations examined (Table 5). Key et al. (1996) suggested that the Efimova/Jacobs schemes perform best. If we consider the modifications to the clear-sky emission characteristics (above), the Efimova/Jacobs and the MC/Jacobs combinations perform better than the Efimova/MC model (Table 6), with Efimova/Jacobs performing the best. The MC cloudy-sky correction for long-wave radiation consistently underestimates fluxes in cloudy skies.

A noticeable trait in the data and the results of Key et al. (1996) is a consistent negative slope (within a 99% confidence interval) in the $L\downarrow_{cld}$ error as the observed flux in Fig. 4 increases (i.e., the estimated flux underestimates real fluxes as the magnitudes of the fluxes increase). This suggests that the cloudy-sky emissivity is too small and needs to be increased. If the cloudy-sky emissivity is increased in MC (from 0.2232 to 0.32) and Jacobs (from 0.26 to 0.275) the results are again different (Table 7 and Fig. 5). The cloudy-sky emissivities of MC and Jacobs were optimized as before by minimizing the MBE for each scheme. After optimizing the cloud-sky emissivities, all of the parametrizations perform well based on the error indices (Table 7), however, the modified MC cloudy-sky formulation relaxes the negative slope (with 95% confidence) in the $L\downarrow_{cld}$ error (Fig. 5) with increasing flux. This is due to the MC cloudy-sky exponential dependence in Eq. (9). The Jacobs cloudy-sky formulation neglects this exponential factor. Very similar results (within a few percent) were obtained using the terrestrial data.

3 SEASONAL TRENDS

The superior parametrizations above and those modified to fit the NOW region were evaluated for seasonal bias (see Section 2c). The Shine $K\downarrow_{clr}$ scheme has a positive seasonal bias (confidence interval of 99%) by slightly underestimating fluxes in the early part of the season and overestimating fluxes in the latter part of the season (Fig. 6). The overestimation in the late season could be, in part, due to the model's inability to represent the increase in atmospheric optical depth associated with rising temperatures and water vapour loading (see also, Leontyeva and Stamnes, 1993; Blanchet and List, 1983).

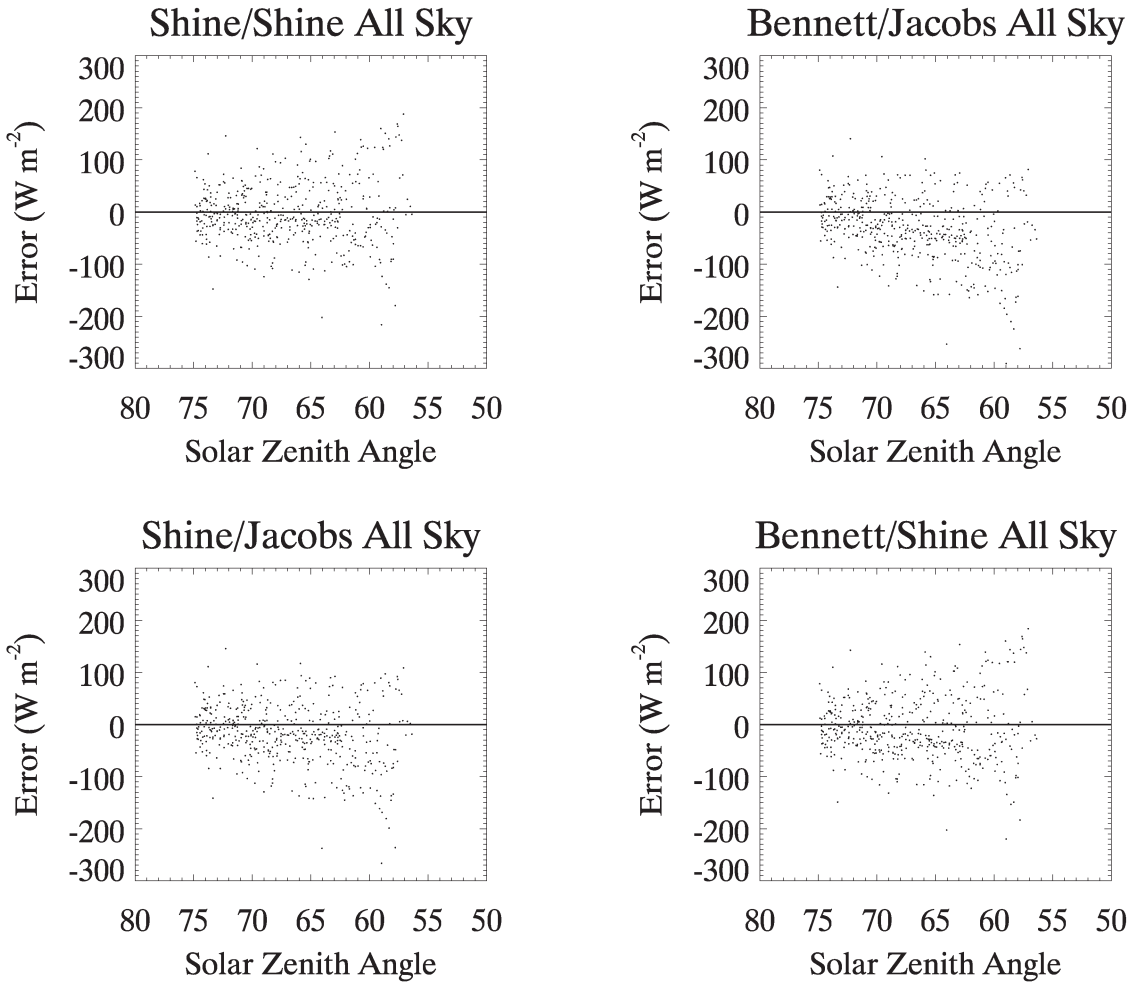

Fig. 3 The all-sky short-wave flux error for four combinations of parametrizations (modelled flux minus the observed flux at Rosse Bay). The first name refers to the clear-sky parametrization used for that combination from Fig. 2.

TABLE 3. Parametrized clear-sky long-wave flux error (estimated flux minus the measured fast-ice flux). Bracketed values are the corresponding ice-breaker results. The mean, mean error and RMSE are in W m^{-2}. The number of observations is also shown.

No. obs = 200(131)	Mean	R^2	Mean Error	RMSE
Observed	197.5(235.4)	–	–	–
MC	209.8(243.9)	0.97(0.80)	12.2(8.5)	7.3(17.8)
Ohmura	192.5(230.6)	0.97(0.80)	–4.9(-4.8)	6.6(17.3)
Efimova	207.9(247.9)	0.98(0.80)	10.4(12.5)	6.1(17.0)

TABLE 4. Parametrized clear-sky long-wave flux error (estimated flux minus the measured fast-ice flux) when altering the emissivity in MC (from 0.7855 to 0.729) and Efimova (from 0.746 to 0.70). Bracketed values are the corresponding ice-breaker results. The mean, mean error and RMSE are in W m^{-2}. The number of observations is also shown.

No. obs = 200(131)	Mean	R^2	Mean Error	RMSE
Observed	197.5(235.4)	–	–	–
MC	197.6(238.0)	0.98(0.81)	0.1(2.7)	5.2(16.7)
Efimova	197.6(242.9)	0.98(0.80)	0.1(7.5)	5.2(17.8)

Integrated total column water vapour using radiosondes launched from the ice-breaker increased from 2 kg m^{-2} in mid-April to 5.5 kg m^{-2} by early May then 9 kg m^{-2} in early June and 11 kg m^{-2} by early July. Surface vapour pressures also increased over the warm season but a de-coupling between the surface and lower troposphere (if it occurred) may affect the results. This is especially important over fast ice in the cold season under inversion conditions where the near-surface temperature and humidity may not represent total column characteristics. Hanafin and Minnett (this issue) utilized results here to further improve the Shine scheme over the polynya in the warm season by increasing the coefficient of the water vapour term. Aerosol effects are unknown since no measurements were available, however, these effects would lead to the most serious errors in the parametrizations (Shine, 1984); the radiative effects of the aerosols being strongly dependent on the atmospheric humidity (e.g., Hänel, 1976) and once again total column variations (Bergin et al.,

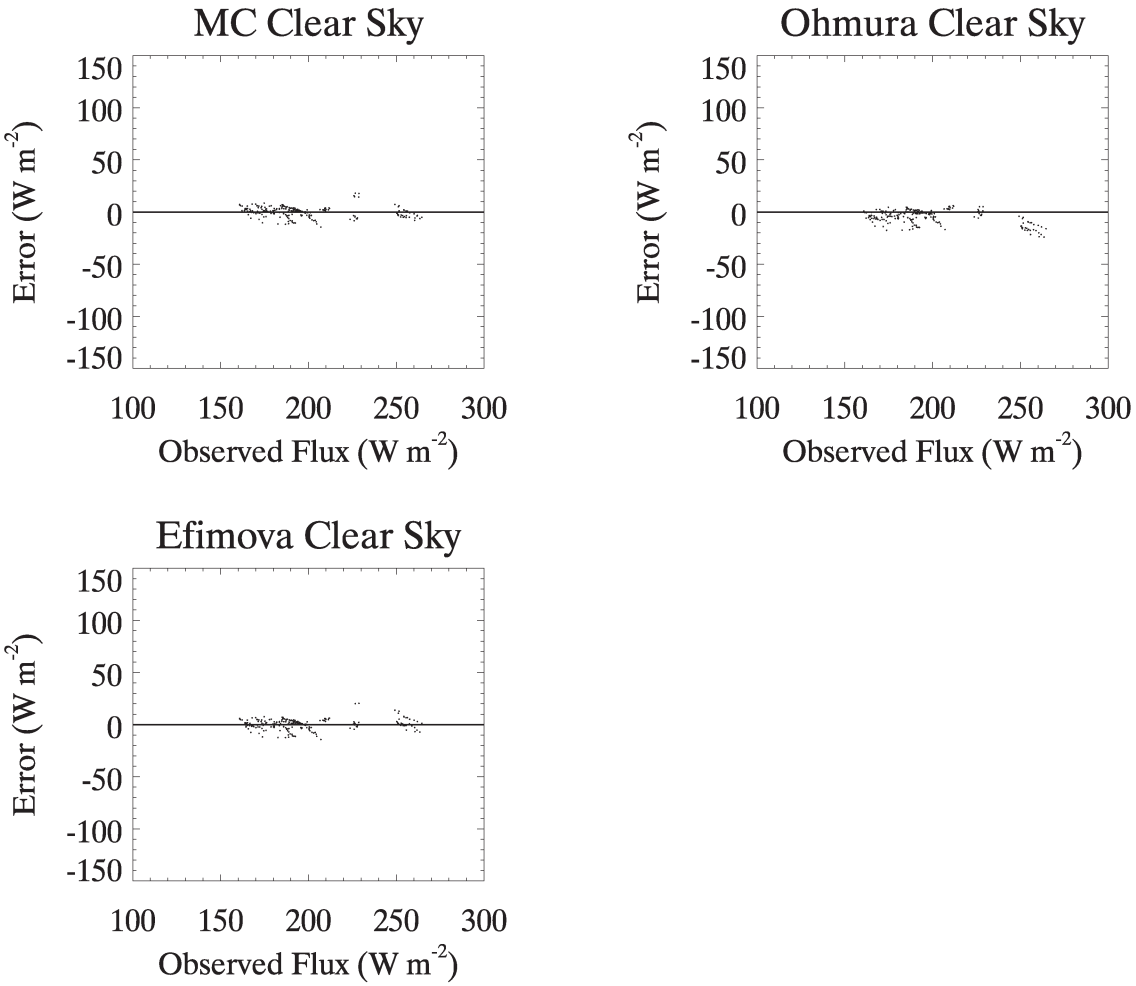

Fig. 4 The clear-sky long-wave flux error (modelled flux minus the observed flux) for the optimized emissivities in MC and Efimova to fit the Rosse Bay data (see text).

TABLE 5. Parametrized all-sky long-wave flux error (estimated flux minus the measured fast-ice flux). Bracketed values are the corresponding ice-breaker results. The mean, mean error and RMSE are in W m^{-2}. The number of observations is also shown.

No. obs = 622(857)	Mean	R^2	Mean Error	RMSE
Observed	231.6(277.8)	–	–	–
MC/MC	238.0(262.8)	0.92(0.73)	6.4(-15.1)	14.9(19.3)
Ohmura/Jacobs	226.1(260.5)	0.89(0.78)	–5.5(-17.3)	16.9(17.6)
Efimova/Jacobs	243.7(280.1)	0.90(0.79)	12.1(2.2)	16.3(17.4)
MC/Jacobs	251.8(282.6)	0.90(0.77)	20.1(4.8)	16.2(18.1)
Efimova/MC	230.4(260.4)	0.92(0.75)	–1.2(-17.4)	14.9(18.4)

TABLE 6. Parametrized all-sky long-wave flux error (estimated flux minus the measured fast-ice flux) when applying the new clear-sky formulations of MC and Efimova from Table 4. The mean, mean error and RMSE are in W m^{-2}. The number of observations is also shown.

No. obs = 622	Mean	R^2	Mean Error	RMSE
Observed	231.6	–	–	–
MC/MC	221.8	0.92	–9.8	15.4
Ohmura/Jacobs	226.1	0.89	–5.5	16.9
Efimova/Jacobs	229.6	0.89	–2.0	16.8
MC/Jacobs	234.6	0.89	2.9	16.9
Efimova/MC	217.1	0.92	–14.5	15.2

TABLE 7. Parametrized all-sky long-wave flux error (estimated flux minus the measured fast-ice flux) when applying the new clear-sky formulations of MC and Efimova from Table 4 and the new cloudy-sky formulation of MC and Jacobs (see text). Bracketed values are the corresponding ice-breaker results. The mean, mean error and RMSE are in W m^{-2}. The number of observations is also shown.

No. obs = 622(857)	Mean	R^2	Mean Error	RMSE
Observed	231.6(277.8)	–	–	–
MC/MC	231.9(265.1)	0.92(0.76)	0.3(–12.7)	13.9(20.3)
Ohmura/Jacobs	228.1(262.6)	0.89(0.78)	–3.5(–15.3)	16.6(17.7)
Efimova/Jacobs	231.7(276.5)	0.90(0.79)	0.1(–1.3)	16.4(18.3)
MC/Jacobs	236.7(278.8)	0.90(0.80)	5.0(0.9)	16.5(17.5)
Efimova/MC	227.1(262.9)	0.93(0.75)	–4.6(–14.9)	13.8(21.0)

2000) that are largely unknown in the Arctic. Radiative transfer models perform well in mid-latitudes (Jing and Cess, 1998) but have not been tested to the same degree in Arctic environments.

The Shine $K\downarrow$ all-sky scheme (Fig. 7) excessively depletes radiation in the early and middle part of the season and not enough in the late season (within a 99% confidence interval). This is likely because of optically thinner clouds during the

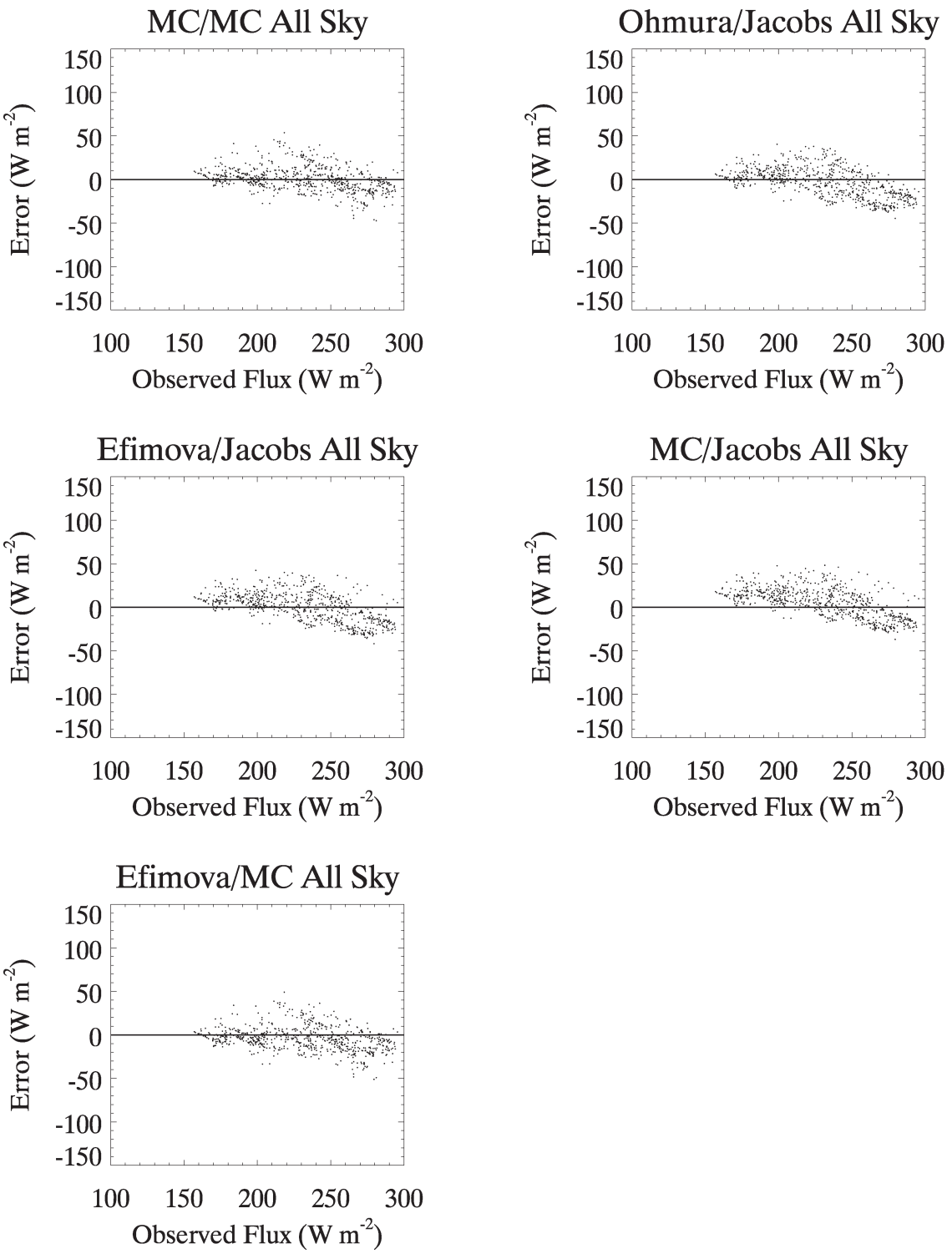

Fig. 5 The all-sky long-wave flux error for five combinations of parametrizations (modelled flux minus the observed flux at Rosse Bay). The first name refers to the clear-sky parametrization used for that combination using the optimized clear-sky emissivities in Fig. 4 and optimized cloudy-sky emissivities of MC and Jacobs to fit the Rosse Bay data (see text).

colder part of the season than in the warmer season. Recall that the Shine model has an inherent clear-sky bias that affects the all-sky calculation. If we decrease the cloud optical depth (from its assumed constant value of 7.0) to 1.0 for $T \leq -20°C$, the all-sky Shine/Shine mean error drops to the Shine clear-sky mean error for the same temperature category. Using the same procedure for $-20°C < T \leq -14°C$, the cloud optical depth becomes 5.5 and stays near 7.0 for

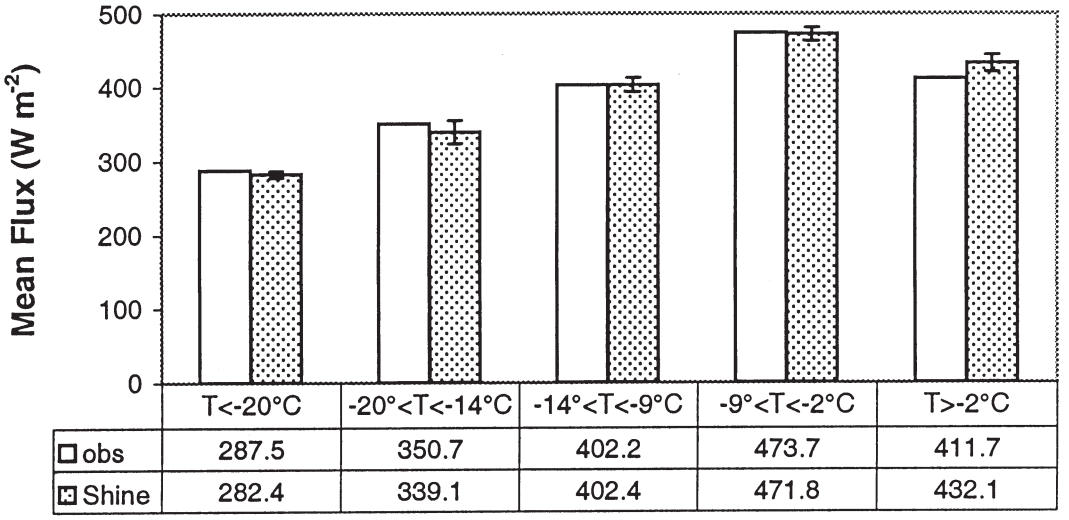

Fig. 6 The short-wave observed and Shine scheme seasonal clear-sky fluxes (W m^{-2}). The RMSE error bars are also shown. The coldest temperature category contained 13 data points, 34 in the next warmest, 48 in the next warmest, 20 in the next warmest and 32 in the warmest category.

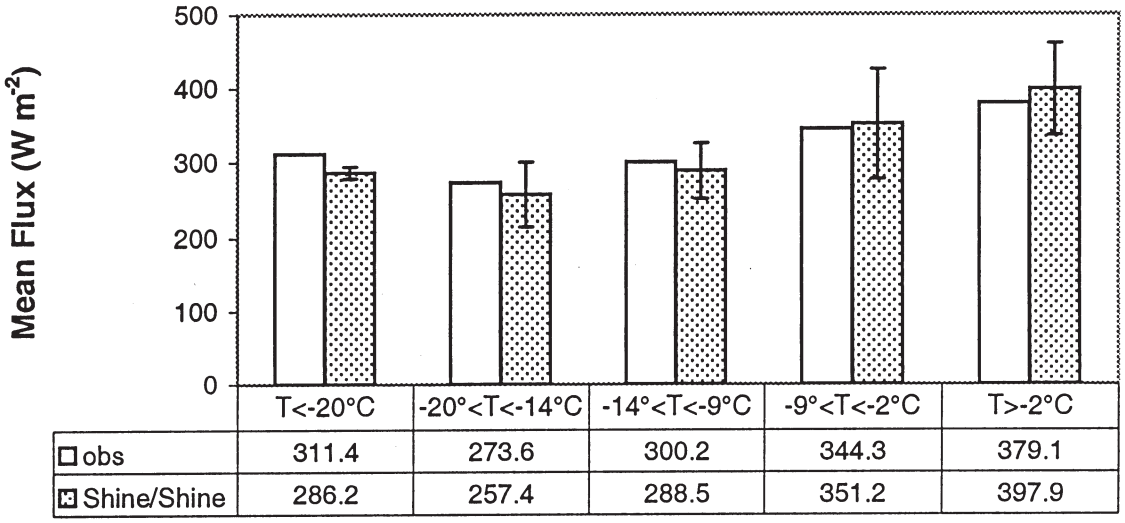

Fig. 7 The short-wave observed and Shine/Shine scheme seasonal all-sky fluxes (W m^{-2}). The RMSE error bars are also shown. The coldest temperature category contained 11 data points, 61 in the next warmest, 156 in the next warmest, 235 in the next warmest and 25 in the warmest category.

warmer temperatures. This suggests an increasing cloud optical depth would improve the $K\downarrow$ all-sky estimates as the warm season approaches. The results are consistent with Curry and Ebert (1992) and Leontyeva and Stamnes (1993) who suggest a cloud optical depth near 7.0 for the warm season. We assume the presence of mid- and upper-level cloud has no seasonal trend when obscured by low cloud during ground observations. Other radiative transfer issues such as solar zenith angle, atmospheric gas variations, 3-D cloud variations, and averaging procedures also affect the results (see for example, Li et al., 1993; Evans, 1998; Arking et al., 1992; Bergin et al., 2000; Barker and Davies, 1992) but cannot be realistically accounted for here. These issues also apply to the ice-breaker results (Section 3b).

The $L\downarrow_{clr}$ seasonal trends of MC (modified) and Efimova (modified) are depicted in Fig. 8. The MC parametrization does not contain a seasonal bias (with 99% confidence). Effimova's scheme contains a slight negative bias (with 99% confidence) early in the season and a positive bias late in the season. The Efimova emissivity was adjusted as in MC, but the vapour pressure dependence in Efimova may introduce other complications.

The $L\downarrow$ all-sky seasonal trends of MC/MC (modified) and Efimova/MC (modified) are depicted in Fig. 9. The MC/MC combination does not contain a seasonal bias (99% confidence). The Efimova/MC combination also did not have a seasonal bias (99% confidence) but contains a consistent negative error similar to that shown earlier in Table 7.

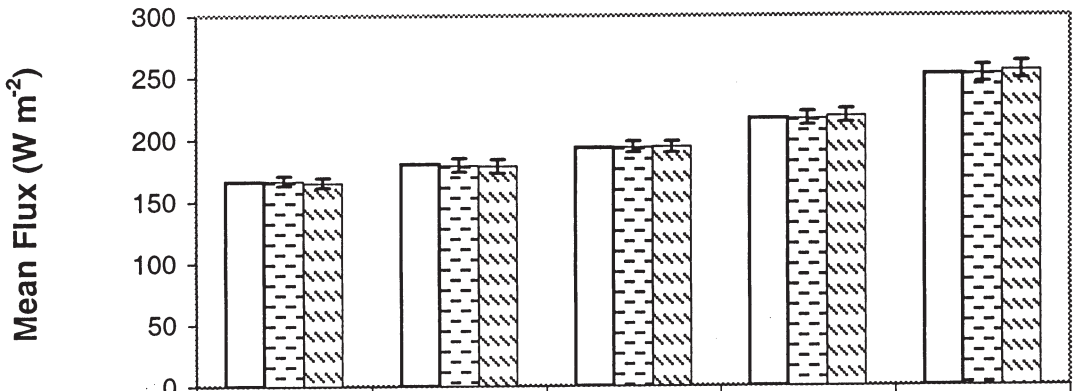

	T<-20°C	-20°<T<-14°C	-14°<T<-9°C	-9°<T<-2°C	T>-2°C
obs	166.1	180.3	193.4	216.8	252.2
MC	166.9	179.4	194	216.8	252.5
Efimova	165.3	178.5	194.1	219	255.4

Fig. 8 The long-wave observed, MC and Efimova schemes seasonal clear-sky fluxes (W m^{-2}). The RMSE error bars are also shown. The coldest temperature category contained 29 data points, 61 in the next warmest, 73 in the next warmest, 21 in the next warmest and 34 in the warmest category.

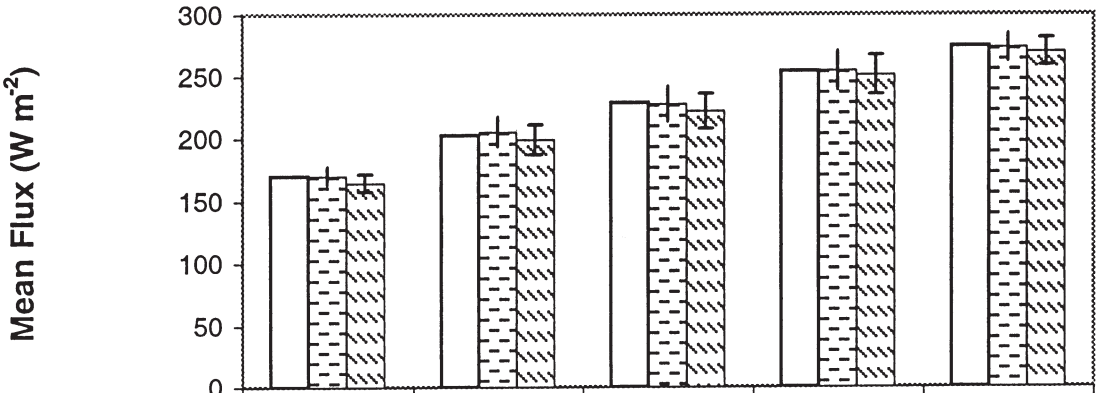

	T<-20°C	-20°<T<-14°C	-14°<T<-9°C	-9°<T<-2°C	T>-2°C
obs	169.9	202.4	228.5	253.9	274.3
MC/MC	170.1	205.4	227.3	254.4	272.8
Efimova/MC	164.3	199	221.6	251	269.6

Fig. 9 The long-wave observed, MC/MC and Efimova/MC schemes seasonal all-sky fluxes (W m^{-2}). The RMSE error bars are also shown. The coldest temperature category contained 34 data points, 139 in the next warmest, 239 in the next warmest, 257 in the next warmest and 28 in the warmest category.

b *Ice-Breaker Platform*

A similar analysis to the last section was conducted on the ice-breaker $K\downarrow$ and $L\downarrow$. All of the different parametrizations were used for the analysis, including the original and modified long-wave schemes. The same seasonal bias analysis used in Section 3a was employed for the ice-breaker data. However, polynya air temperatures were warmer than the fast-ice region, thus, only three temperature categories of air temperature were used.

1 INCIDENT SHORT-WAVE FLUXES

The $K\downarrow_{clr}$ results show that the Shine and Bennett schemes perform worst within the polynya relative to the fast-ice and terrestrial sites (Table 1). Note that all ice-breaker data in the Tables appear in brackets. The schemes overestimate fluxes with an RMSE 2–3 times larger than the fast-ice results. Both the Shine and Bennett schemes contained a more pronounced positive seasonal bias (with 99% confidence) (Fig. 10). The general overestimation of clear-sky fluxes is likely due to

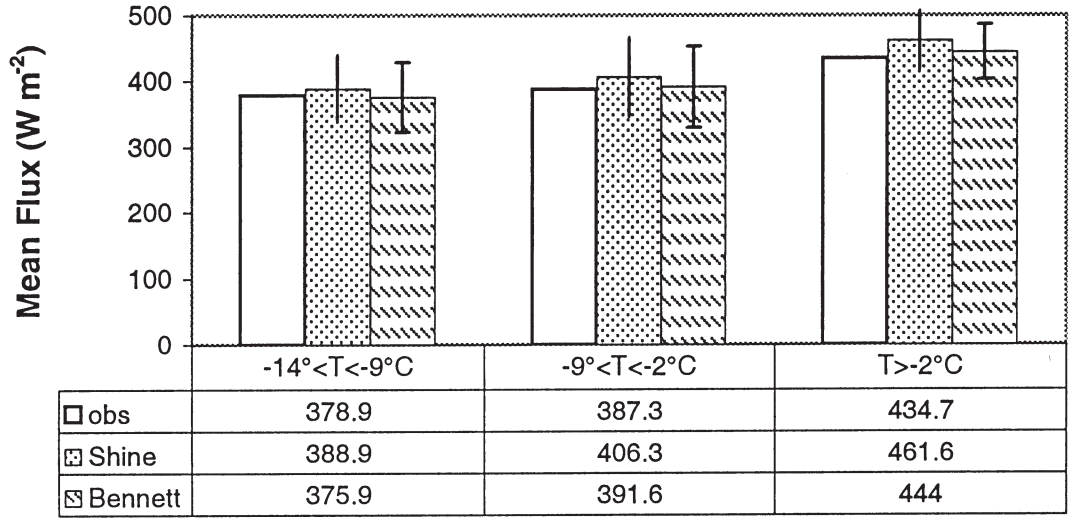

Fig. 10 As in Fig. 6 except for the ice-breaker. The coldest temperature category contained 7 data points, 26 in the next warmest, and 71 in the warmest category.

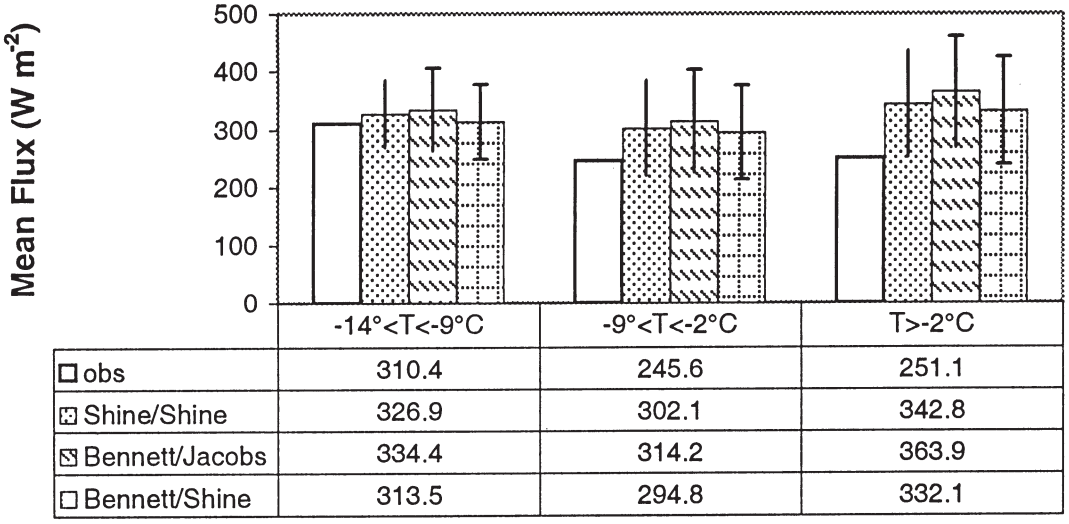

Fig. 11 As in Fig. 7 except for the ice-breaker. The coldest temperature category contained 9 data points, 139 in the next warmest, and 407 in the warmest category.

greater total column water vapour than originally intended for the schemes, especially for the marine environment. Hanafin and Minnett (this issues) have corrected for this in the Shine scheme.

The ice-breaker results for $K\downarrow$ all-sky show a larger RMSE relative to the clear-sky case (Table 2). The mean errors and RMSE in the ice-breaker results are also much greater than the fast ice. The cause is likely the result of marine clouds being optically thicker than the fast-ice environment. There is a positive seasonal bias in the ice-breaker-derived fluxes where fluxes are overestimated more so as the ambient temperatures increase (with 99% confidence) (Fig. 11). If cloud optical depth is increased from 7.0 to 9.0 for $-14°C < T \leq -9°C$, the all-sky Shine/Shine mean error dropped to the Shine clear-sky mean error for the same temperature category. Similarly, for $-9°C < T \leq -2°C$, the cloud optical depth increases to 14 and further increases to 20 for $T > -2°C$. These optical depths are consistent with typical Arctic stratus clouds (Herman and Curry, 1984; Leontyeva and Stamnes, 1993). This is also different than the fast-ice site where an optical depth of 7.0 works well for warmer temperatures. Once again we assume there is no seasonal bias in the presence of mid- and upper-level cloud when they are obscured by low cloud during ground observations.

2 INCIDENT LONG-WAVE FLUXES

The MC and Efimova $L\downarrow_{clr}$ overestimate smaller fluxes (i.e., $L\downarrow < 240$ W m^{-2}), consistent with results from Table 3. The error terms are improved when applying the fast-ice adjustment to the MC and Efimova schemes. Both the MC and

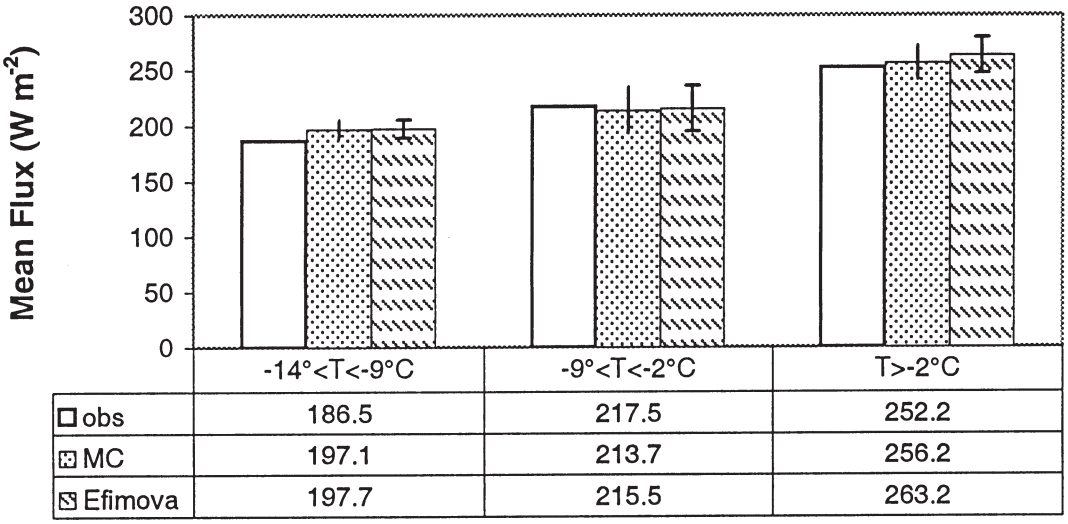

	-14°<T<-9°C	-9°<T<-2°C	T>-2°C
obs	186.5	217.5	252.2
MC	197.1	213.7	256.2
Efimova	197.7	215.5	263.2

Fig. 12 As in Fig. 8 except for the ice-breaker. The coldest temperature category contained 15 data points, 35 in the next warmest, and 81 in the warmest category.

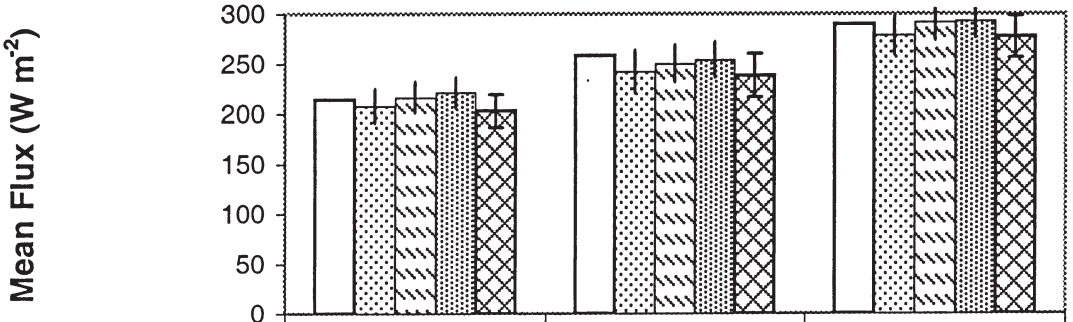

	-14°<T<-9°C	-9°<T<-2°C	T>-2°C
obs	214.5	258.1	289.9
MC/MC	207.7	241.8	278.4
Efimova/Jacobs	216.3	250	291.4
MC/Jacobs	221.2	253.8	292.8
Efimova/MC	203.1	238.3	277.1

Fig. 13 As in Fig. 9 except for the ice-breaker. The coldest temperature category contained 29 data points, 256 in the next warmest, and 572 in the warmest category.

Efimova schemes do not contain the seasonal bias (with 99% confidence) over the polynya (Fig. 12). Recall that a slight positive bias was found in the Efimova scheme for the fast ice.

The ice-breaker $L\downarrow$ all-sky errors improve when using the modified schemes from Section 3a (comparing Tables 5 and 7). However, there is more variation in the mean errors than the fast-ice results with slightly larger RMSE and smaller R^2 (Table 7). Note the MBE is more negative than the fast-ice site (Table 7). This may be due to: 1) warmer mean ambient temperatures (and later data collection dates) accompanying the ice-breaker data, 2) the cloud emissivity needing to be increased in a full marine environment (with optically thicker clouds) compared to the fast-ice regime, and 3) cloud base heights being lower in the marine environment. The first reason can be ruled out since the ice-breaker mean error is consistently more negative than the fast-ice mean errors for similar temperatures and data collection dates. This suggests that the cloud emissivity needs to be increased for the marine schemes and/or the cloud base heights were lower in the marine environment. The $K\downarrow$ all-sky results suggest a greater cloud optical depth in the polynya implying higher within-cloud precipitable water and in turn higher cloud emissivity. A higher cloud emissivity is required to match the parametrization schemes with measured flux density within the polynya. Cloud base heights would also contribute to the differences.

Combinations using the Jacobs cloudy-sky scheme are more consistent on a seasonal basis and have the smallest mean errors. The Jacobs scheme was developed from data during the warm season to early winter (June–December) that may contribute to its better performance in a marine setting. The modified MC/MC and Efimova/MC scheme combinations were best in the fast-ice and terrestrial sites but would need to be further adjusted for the marine data. Hanafin and Minnett (this issue) have further improved the MC/MC $L\downarrow$ all-sky scheme in the polynya setting.

Given that the open water of the polynya is the major source of atmospheric water vapour in the area, it is to be expected that the water vapour burden and distribution will show differences between open water and land. The dominant wind direction in the area is from the NNW (Hanesiak, 1998) and so the terrestrial and fast-ice data are predominantly under the influence of winds blowing over the land surface of Ellesmere Island; the ice-breaker measurements include a wide range of conditions, in terms of sea-ice cover and open water, that are unparametrized in the formulations used here. In particular the water vapour distribution is a strong function of fetch over open water for situations of off-ice winds. This has the potential to not only increase the variability of the parametrization uncertainties, but also to introduce bias errors.

While there are convincing physical reasons to explain the observed increases in uncertainty in the parametrized fluxes when compared to ship-based measurements, as opposed to measurements from fixed platforms, there is always the possibility that these are not a result of shortcomings in the parametrizations, but of flawed measurements. Of obvious concern is ship motion. In an attempt to reduce ice-breaker tilting of the radiometers, they were mounted on gimbals. This means that, on average, they are level; but at any moment may be tilted as a result of ship motion. Observations showed that in most cases the amplitude of the oscillation was only a few degrees, with some infrequent large amplitudes when the ship was breaking thick ice. The consequence of tilt is severe in the $K\downarrow$ measurements, as this has the effect of changing the apparent Z. However, while mean tilts can lead to significant errors, especially in clear skies, small-amplitude oscillating tilts do not significantly degrade the data (MacWhorter and Weller, 1991). The $L\downarrow$ measurement is inherently less sensitive to tilts of the pyrgeometer, but there is an error source caused by the temperature contrast between the sky and land, sea or ice. As the pyrgeometer tilts, it receives radiation from a warmer source, below the horizon, than the sky. Oscillating tilts do not cancel out but combine to produce a positive bias error. The effect of this would be to make a parametrization of $L\downarrow$ appear to predict lower fluxes compared to the measurements, and this is indeed observed in some cases. Such an effect would be indistinguishable from the environmental factors discussed above. Clearly the issue of making accurate $K\downarrow$ and $L\downarrow$ measurements from ships requires further attention, but it is certainly not clear that these instrumental effects are of sufficient magnitude to dominate the error characteristics of the results discussed here.

4 Conclusions

Our purpose in this paper was to assess the performance of simple incident short-wave and long-wave radiation parametrizations used in several thermodynamic ice models and to investigate any inherent temporal and/or spatial biases inherent in these parametrizations. The parametrized fluxes were compared to in situ measurements made over a terrestrial site, landfast ice site and from the ice-breaker during the 1998 International NOW Polynya project. However, limitations of the input data and largely unknown total column atmospheric conditions can affect the results of the analysis.

The fast-ice and terrestrial regimes showed very similar characteristics (within ± 2%) due to their close geographic proximity and snow-covered surfaces. Differences arose when comparing the terrestrial/fast-ice results to the marine environment sampled by the ice-breaker.

The fast-ice preferred $K\downarrow_{clr}$ scheme was Shine (1984) which contained no solar zenith angle (Z) bias, unlike the scheme of Bennett (1982). However, the Shine scheme contained a positive seasonal bias where it underestimated fluxes in the cold season and overestimated fluxes in the warm season. The positive bias was more dramatic in the marine data. Hanafin and Minnett (this issue) built on these results to improve the Shine clear-sky scheme over the polynya. Likely causes and errors for the differences were offered.

The preferred fast-ice $K\downarrow$ all-sky combination scheme was the Shine (1984) clear-sky and Shine (1984) cloudy-sky. The Jacobs (1978) cloudy-sky scheme depleted too much radiation. The Shine cloudy-sky scheme depletes too much radiation in the colder season and not enough in the warm season, especially in the marine warm season. An improved implementation of the Shine scheme was made by varying the cloud optical depth. If cloud optical depth is allowed to vary seasonally from 1 to 7 in the fast-ice environment (late March to early June) and 9 to 20 in the marine setting (early May to mid-July), the Shine cloudy-sky fluxes become closer to observed values. These optical depths are within the limits of Arctic clouds (Herman and Curry, 1984; Shine et al., 1983; Shine, 1984). Sea-ice models should allow for seasonal cloud optical depth variations with respect to incident short-wave radiation, even if they are used in a climatological sense.

The preferred fast-ice $L\downarrow_{clr}$ parametrization is Maykut and Church (1973) after adjusting (decreasing) the clear-sky emissivity to account for a less emissive atmosphere at colder temperatures in the NOW project. This correction was sufficient for the marine conditions. The MC scheme did not contain a seasonal bias once this correction was made.

The preferred fast-ice $L\downarrow$ all-sky combination was the MC clear-sky and the MC cloudy-sky. We increased the cloudy-sky emissivity to account for underestimations when clouds were present which also alleviated a slight seasonal bias. The MC exponential dependence of cloud fraction (Eq. 9) was also found to be important.

Different $L\downarrow$ all-sky results were found for the marine environment. Overall, the ice-breaker consistently had more negative mean errors compared to the fast-ice site. This was not

due to warmer ambient marine temperatures. The all-sky short-wave flux results suggested the marine environment had greater cloud optical depths compared to the fast-ice and terrestrial sites and is consistent with the long-wave results where a higher cloud emissivity may be required; although cloud base height differences could also be a factor. The Jacobs cloudy-sky scheme is more consistent on a seasonal basis and has the smallest mean errors. The MC cloudy-sky scheme was further improved by Hanafin and Minnett (this issue) for the marine setting.

We recommend using: 1) our modified MC $L\downarrow$ clear and cloudy-sky schemes for a polynya fast-ice and terrestrial environment, 2) our modified Efimova/Jacobs or MC/Jacobs schemes for the Arctic marine environment, and 3) our modified Efimova/Jacobs scheme for application to all three environments simultaneously since it was the most consistent for this purpose. The modified MC and Efimova $L\downarrow_{clr}$ formulations are, respectively:

$$L\downarrow_{clr} = 0.729\ \sigma\ Ta^4. \tag{10}$$

$$L\downarrow_{clr} = \sigma\ Ta^4\ (0.7 + 0.0066\ ea). \tag{11}$$

The modified MC and Jacobs $L\downarrow$ all-sky formulations are, respectively:

$$L\downarrow_{all} = L\downarrow_{clr}\ (1 + 0.32\ c^{2.75}). \tag{12}$$

$$L\downarrow_{all} = L\downarrow_{clr}\ (1 + 0.275\ c). \tag{13}$$

Acknowledgements

Appreciation is extended to Dr. Rick Marsden (Royal Military College, Kingston ON) for providing ice-breaker (CCGS *Pierre Radisson*) relative humidity data and to all of the data collection personnel who participated in the 1998 NOW Polynya Sea Ice/Climate Dynamics sub-group. We also wish to thank the Captains, officers and crew of the CCGS *Pierre Radisson* and the Polar Continental Shelf Project for logistical support. Gratitude is also extended to Wayne Chan and Oksana Banias (University of Manitoba), Jennifer Hanafin and Erica Key (University of Miami) for at-sea support; and Carrie Wootton and Robert Jones (University of Miami) for help with data processing. This research was financially supported by a grant from the Meteorological Service of Canada under the CRYSYS project (Dr. B. Goodison, PI), a Natural Sciences and Engineering Research Council grant, and an Office of Naval Research Grant (#N00014-94-1-03-86) each to DGB. Research was also funded through grants from the National Science Foundation Office of Polar Programs (OPP9708045) and the National Aeronautics and Space Administration (NAG56577) to PJM.

References

ARKING, A.; O.M. IZAKOVA and Y.E.M. FEYGEL'SON. 1992. Use of satellite, ground, and aerological data for calculating IR fluxes. *Atmos. Oceanic Phys.* **28**: 283–287.

BARBER, D.G.; R. MARSDEN, P. MINNETT, G. INGRAM and L. FORTIER. 2001. Physical Processes within the North Water (NOW) Polynya. ATMOSPHERE-OCEAN, **39**: 163–166.

———, and S.V. NGHIEM. 1999. The role of snow on the thermal dependence of backscatter over sea ice. *J. Geophys. Res.* **104(C11)**: 25,789–25,803.

BARKER, H.W. and J.A. DAVIES. 1992. Solar radiative fluxes for stochastic, scale-invariant broken cloud fields. *J. Atmos. Sci.* **49**: 1115–1126.

BENNETT, T.J. 1982. A coupled atmosphere-sea ice model study of the role of sea ice in climatic predictability. *J. Atmos. Sci.* **39**: 1456–1465.

BERGIN, M.H.; S.E. SCHWARTY, R.N. HALTHORE, J.A. ORGEN and D.L. HLAVKA. 2000. Comparison of aerosol optical depth inferred from surface measurements with that determined by sun photometry for cloud-free conditions at a continental U.S. site. *J. Geophys. Res.* **105(D5)**: 6807–6816.

BLANCHET, J.-P. and R. LIST. 1983. Estimation of optical properties of Arctic haze using a numerical model. ATMOSPHERE-OCEAN, **21**: 444–465.

CARSEY, F. 1992. Microwave Remote Sensing of Sea Ice. American Geophysical Union. 1993. Geophysical Monograph #68. 462 pp.

CURRY, L.A. and E.E. EBERT. 1992. Annual cycle of radiative fluxes over the Arctic Ocean: sensitivity to cloud optical properties. *J. Clim.* **5**: 1267–1280.

EBERT, E.E. and J.A. CURRY. 1993. An intermediate one-dimensional thermodynamic sea ice model for investigating ice-atmosphere interactions. *J. Geophys. Res.* **98(C6)**: 10,085–10,109.

EFIMOVA, N.A. 1961. On methods of calculating monthly values of net long-wave radiation. *Meteorol. Gidrol.* **10**: 28–33.

EVANS, K.F. 1998. The spherical harmonics discrete ordinate method for three-dimensional atmospheric radiative transfer. *J. Atmos. Sci.* **55**: 429–446.

FLATO, G.M. and R.D. BROWN. 1996. Variability and climate sensitivity of land-fast Arctic sea ice. *J. Geophys. Res.* **101(C10)**: 25767–25777.

HANAFIN, J.A. and P.J. MINNETT. 2001. Cloud forcing of surface radiation in the North Water Polynya. ATMOSPHERE-OCEAN, **39**: 239–255.

HÄNEL, G. 1976. The properties of atmospheric aerosol particles as functions of the relative humidity at thermodynamic equilibrium with the surrounding moist air. *Adv. Geophys*. **19**: 73–188.

HANESIAK, J.M. 1998. Historical Perspective. *In*: NOW'98 Sea Ice/Climate Dynamics Subgroup Field Summary, Papakyriakou, T.N., C.J. Mundy and D.G. Barber (Eds) Centre for Earth Observations Science, Department of Geography, University of Manitoba, CEOS tech 98-8-2, pp. 15–20.

———; D.G. BARBER and G.M. FLATO. 1999. The role of diurnal processes in the seasonal evolution of sea ice and its snow cover. *J. Geophys. Res.* **104(C6)**: 13593–13603.

HERMAN, G.F. and J.A. CURRY. 1984. Observational and theoretical studies of solar radiation in Arctic stratus clouds. *J. Clim. Appl. Meteorol.* **23**: 5–24.

IPCC (INTERGOVERNMENTAL PANEL ON CLIMATE CHANGE). 1996. Climate Change: The IPCC Assessment. J.T. Houghton, G.J. Jenkens and J.J. Ephraums (Eds) Cambridge University Press, Cambridge, U.K. 572 pp.

JACOBS, J.D. 1978. Radiation climate of Broughton Island, energy budget studies in relation to fast-ice breakup processes in Davis Strait. R.G. Barry and J.D. Jacobs (Eds), Occas. Pap. 26. Inst. Of Arctic and Alp. Res., Univ. of Colorado, Boulder. pp. 105–120.

JEZEK, K.C.; D. PEROVICH, K.M. GOLDEN, C. LUTHER, D.G. BARBER, P. GOGINENI, T. GRENFELL, A. JORDAN, C. MOBLEY, S. NGHIEM and R. ONSTOTT. 1998. A broad Spectral, Interdisciplinary Investigation of the Electromagnetic Properties of Sea Ice. *IEEE Trans. Geosci. Remote Sens. ONR ARI special issue*. **36(5)**:1633–1641.

JING, X. and R.D. CESS. 1998. Comparison of atmospheric clear-sky shortwave radiation models to collocated satellite and surface measurements in Canada. *J. Geophys. Res.* **103(D22)**: 28817–28824.

KEY, J.R.; R.A. SILCOX and R.S. STONE. 1996. Evaluation of surface radiative flux parameterizations for use in sea ice models. *J. Geophys. Res.* **101**: 3839–3849.

LATIMER, J.R. 1972. Radiation Measurement. Technical manual series No. 2, International Field Year for the Great Lakes. National Research Council of Canada. 53 pp.

LEONTYEVA, E. and K. STAMNES. 1993. Estimations of cloud optical thickness from ground-based measurements of incoming solar radiation in the Arctic. *J. Clim.* **7**: 566–578.

LI, Z.; H.G. LEIGHTON, K. MASUDA and T. TAKASHIMA. 1993. Estimation of SW flux absorbed at the surface from TOA reflected flux. *J. Clim.* **6**: 317–330.

MACWHORTER, M.A. and R.A. WELLER. 1991. Error in measurements of incoming shortwave radiation made from ships and buoys. *J. Atmos. Oceanic Technol*. **8**: 108–117.

MASLANIK, J.A.; J. KEY and A.S. SCHWEIGER. 1995. Cloud amount radiation: Effects of climatology and method on Arctic sea ice simulations. *In*: Proc. 4th Conf. On Polar Meteorol. and Oceanog., Dallas, TX, January 1995. Am. Meteorol. Soc.

MAYKUT, G.A. and P.E. CHURCH. 1973. Radiation climate of Barrow, Alaska, 1962–66. *J. Appl. Meteorol.* **12**: 620–628.

MINNETT, P.J. 1999. The influence of solar zenith angle and cloud type on cloud radiative forcing at the surface in the Arctic. *J. Clim.* **12**: 147–158.

MORITZ, R.E. and D.K. PEROVICH (Eds). 1998. SHEBA, A Research Program on the Surface Heat Budget of the Arctic Ocean, Science Plan, Rep. No. 5, U. of Washington, 64 pp.

OHMURA, A. 1981. Climate and energy balance of the Arctic tundra. Zurcher Geogr. Schr 3, Geogr. Inst., Zurich, Switzerland. 448 pp.

PARKINSON C.; D. CAVALIERI, P. GLOERSEN, H. ZWALLY and J. COMISO. 1999. Arctic sea ice extents, areas and trends, 1978–1996. *J. Geophys. Res*. **104(C9)**: 20837–20856.

PHILIPONA, R.; C. FROHLICH and C.H. BETZ. 1995. Characterization of pyrgeometers and the accuracy of atmospheric long-wave radiation measurements. *Appl. Optics*, **34(9)**: 1598–1605.

ROTHROCK, D.A.; Y. YU and G.A. MAYKUT. 1999. Thinning of the Arctic Sea ice Cover. *Geophys. Res. Lett*. **26**: 3469–3472.

SHINE, K.P. 1984. Parameterization of short-wave flux over high albedo surfaces as a function of cloud thickness and surface albedo. *Q. J. R. Meterol. Soc.* **110**: 747–764.

———; A. HENDERSON-SELLERS and R.G. BARRY. 1983. Albedo-climate feedback: The importance of cloud cryosphere variability. In: *New Perspectives in Climate Modeling.* A. Berger and C. Nicolis (Eds), Elsevier, New York, NY. 245 pp.

WALSH, J.E.; W.L. CHAPMAN and T. SHY. 1996. Recent decrease of sea level pressure in the central Arctic. *J. Clim.* **9**: 480–486.